Supportive Information

Ultra-Low Nickel-Doped Copper Aerogels as Highly Efficient and Stable Electrocatalyst for the Formic Acid Oxidation Reaction

Henok Tibebu Weldemichael[1], Amare Aregahegn Dubale[1,*], Mekonnen Abebayehu Desta[2], Taame Abraha Berhe[3,4], Girum Ayalneh Tiruye[1], Chu-Chen Chueh[3], Yonas Chebude[2], Hao-Wei Yu[3]

[1]Center for Material Science and Engineering, College of Natural and Computational Science, Addis Ababa University, Addis Ababa 1176, Ethiopia

[2]Department of Chemistry, College of Natural and Computational Sciences, Addis Ababa University, Addis Ababa 1176, Ethiopia

[3]Department of Chemical Engineering, National Taiwan University, Taipei, Taiwan, P.O. Box 10617 Taipei, Taiwan

[4]Department of Chemistry, College of Natural and Computational Sciences, Adigrat University, Adigrat, P. O. Box 50, Ethiopia

*Corresponding authors email: amare.aregahegn@aau.edu.et (Amare Aregahegn Dubale)

ORCID: 0000-0002-7674-5709

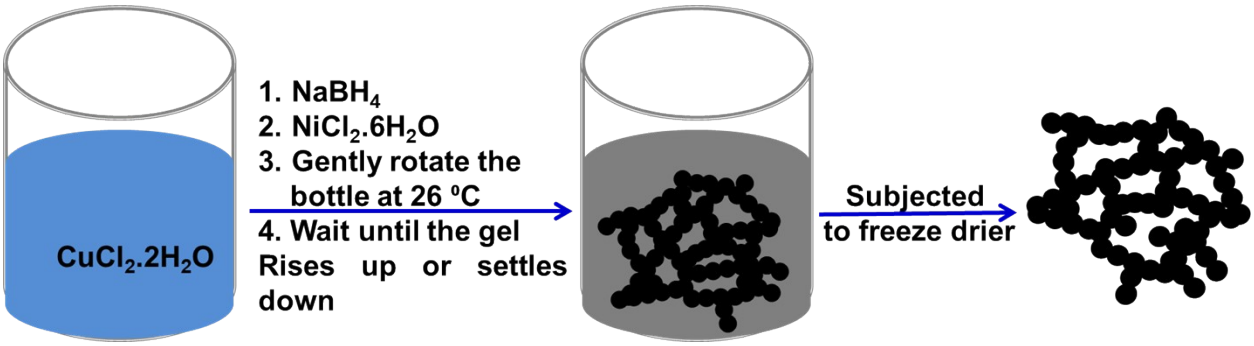

Figure S1. Preparation of Nikel-doped copper aerogels

Table S1: **Molar ratio of Cu and Ni in the Cu_xNi_y aerogels obtained using ICP and XPS.**

Aerogel name	Cu/Ni precursor molar ratio	ICP	XPS		
		Cu/Ni (%)	Cu_2O/Cu (%)	Cu/Ni (%)	$Ni(OH)_2$/Ni (%)
Cu	100/0	100/0	30.2/69.8	100/0	-
$Cu_{98}Ni_2$	98/2	98/2	31.8/68.2	96/4	87.2/12.8
$Cu_{95}Ni_5$	95/5	95/5	31.5/68.5	94/6	88.6/11.4
$Cu_{93}Ni_7$	93/7	92/8	32.3/66.7	90/10	90.4/9.6
Ni	0/100	0/100	-	0/100	91.3/8.7

Table S2. Electrochemical active surface area for different electrodes, attained by averaging the values from the linear relationship between anodic and cathodic peak currents and the square root of the scan rate.

Aerogel name	ECSA obtained using I_{pa} value (cm^2)	ECSA obtained using I_{pc} value (cm^2)	Average ECSA (cm^2)
Cu	0.114	0.183	0.184
$Cu_{98}Ni_2$	1.190	1.455	1.323
$Cu_{95}Ni_5$	0.476	0.608	0.542
$Cu_{92}Ni_8$	0.476	0.661	0.569
Ni	0.108	0.167	0.146

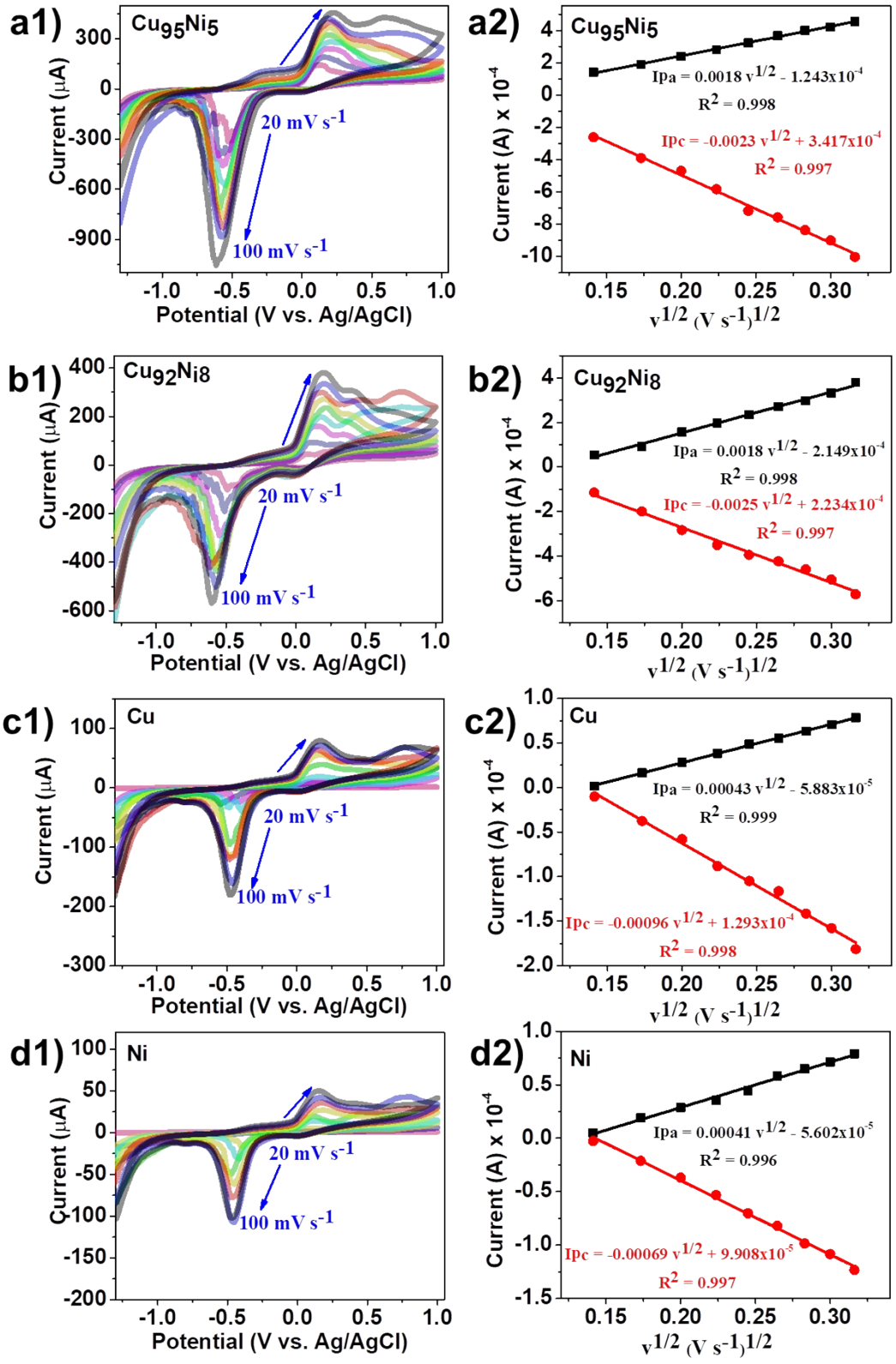

Figure S2. (a1-d1) CV curves of $Cu_{95}Ni_5$, $Cu_{92}Ni_8$, Cu and Ni, respectively in 0.1 M KCl containing 5.0 mM $[Fe(CN)6]^{3-/4-}$ at increasing potential scan rates (20, 30, 40, 50, 60, 70, 80, 90

and 100), and (a2-d2) linear fitting of the anodic and cathodic peak currents to the square roots of the scan rates.

Scherrer equation was employed to determine the relative crystalline size:

$$D = \frac{K\lambda}{\beta cos\theta} \quad (1)$$

where D is relatively grain size, K is Scherrer constant which is 0.9, λ is the wavelength of the X-ray beam which is 1.5406 nm, β is the full width at half maximum (FWHM) of the peak at 2θ values of 31.7˚ and θ the Bragg angle.

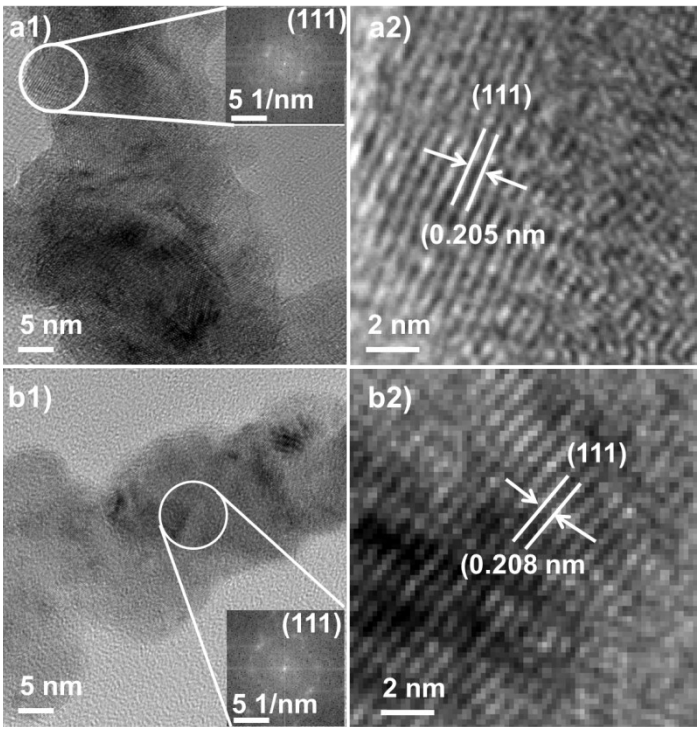

Figure S3. HRTEM images of a) pure Cu aerogel and b) $Cu_{98}Ni_2$ aerogels. The inset in Figure S7 is the FFT at selected regions

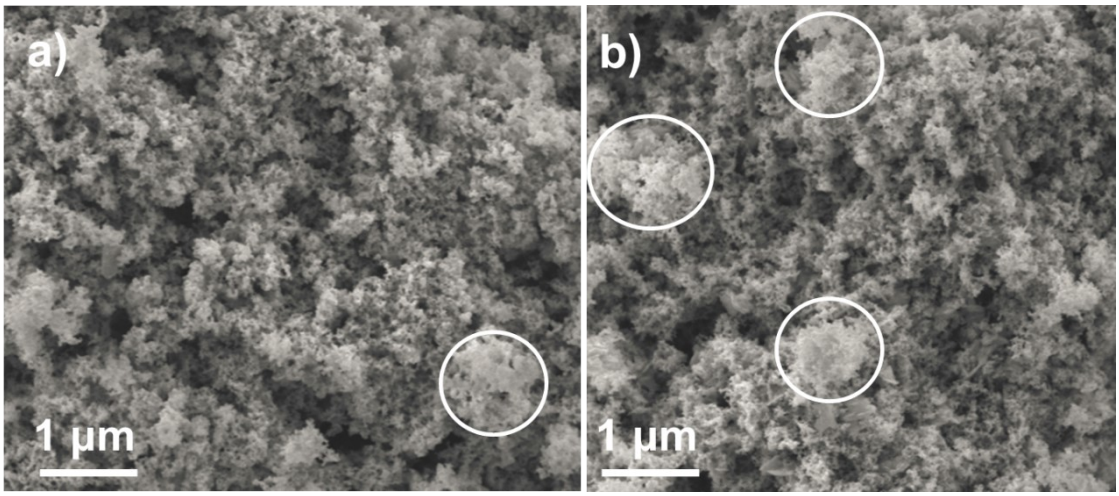

Figure S4. SEM images of $Cu_{95}Ni_5$ (a) and $Cu_{92}Ni_8$ (b) aerogels

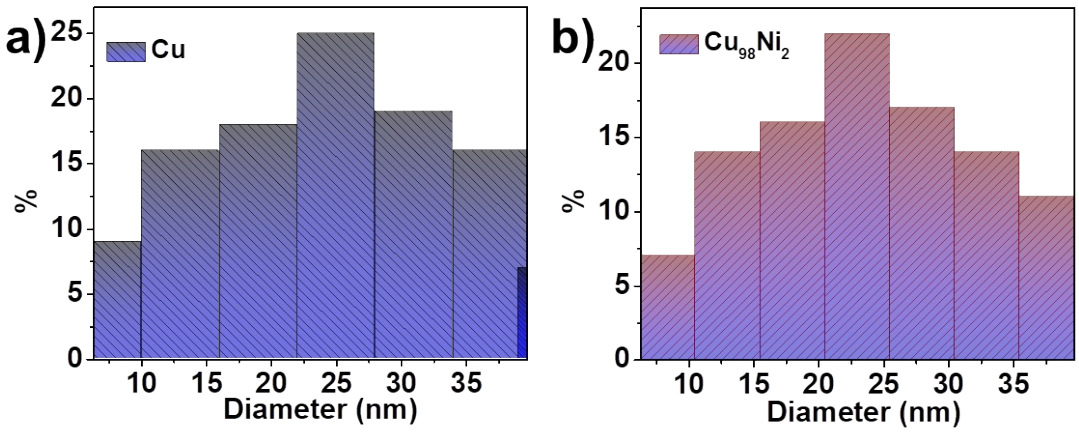

Figure S5. Histograms showing the diameter distribution of nanowire networks in the Cu (a) and $Cu_{98}Ni_2$ aerogels (b). The average diameters of the nanowires were found to be 25 nm, 23 nm, respectively.

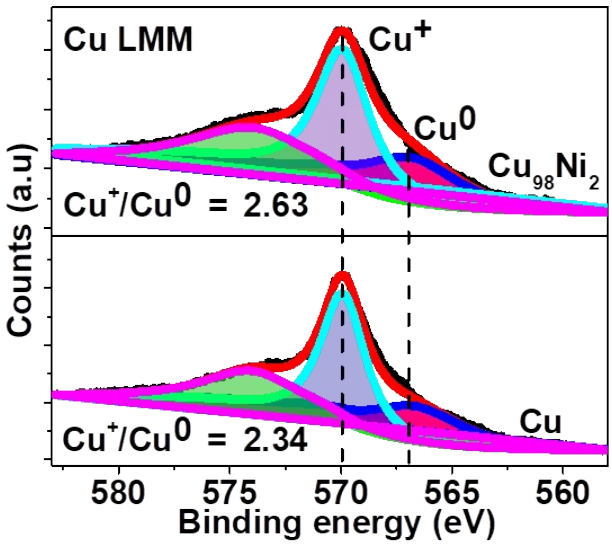

Figure S6. Cu LMM Auger spectra of the pure Cu and $Cu_{98}Ni_2$ aerogel samples.

Table S3. A quantitative comparison of the doping ratio with those reported for similar catalysts to substantiate the claim of "ultra-low" content.

S.N	Ultralow Catalyst system	dopant	Dopant content	Electrocatalysis system	Ref.
1	Ru-Co)Ox-400	Ru	2.0%	Water oxidation	[1]
2	$Ni_{98.1}Ru_{1.9}$	Ru	1.9 %	PEMWE	[2]
3	Fe(III) -Ni_3S_2/NF	Fe(III)	2.1%	Enhanced OER	[3]
4	Pd5-$(C_{12}H_{25}S)_{13}$ nanoclusters	Pd5	2%	ORR and Ethanol oxidation reaction	[4]
5	Pt -$(Nb–Ti)_2AlC$	Pt	3%	Low temperature fuel cell application	[5]
6	Ni on mesoporous SiO_2	Ni	1.8%	Hydrodeoxygenation of palmitic acid	[6]
7	$Cu_{98}Ni_2$	Ni	2%	Formic acid oxidation reaction	This study

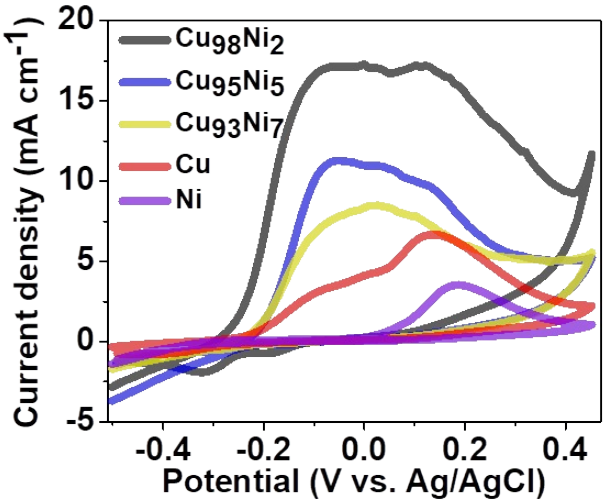

Figure S7. CV curves of Cu, Ni, $Cu_{98}Ni_2$, $Cu_{95}Ni_5$ and $Cu_{92}Ni_8$ in 1 M KOH at scan rate of 50 mV s^{-}.

Then, overpotential is defined as the difference between the applied electrode potential and the thermodynamic potential for the same reaction on the same reference scale.

$$\eta = E_{applied} - E_{thermodynamic} \quad (2)$$

As reported in the literature, the standard potential for the oxidation of formic acid ranges from −0.17 V to −0.25 V vs. SHE.[7] These values correspond to 0.656 V to 0.576 V vs. RHE at a pH of 14, based on the equation $E_{RHE} = E_{SHE} + 0.059 \times pH$.[8]

The anodic half-reaction and the standard potential for the oxidation of formic acid or formate in a basic medium (e.g. 1 M KOH solution) can be expressed as follows[9]:

$HCOO^- + OH^- \rightarrow CO_2 + H_2O + 2e^-$: standard potential ($E^o$) = 0.639 V vs. RHE. Using this half-reaction, we can also calculate the standard potential for the oxidation of formic acid by using the standard Gibbs free energies obtained from thermodynamic tables.

Table S4. Standard Gibbs free energies values from thermodynamic tables.

Species	$\Delta G°f$ (kJ mol^{-1})
$HCOO^-$	−351
OH^-	−157
CO_2	−394
H_2O	−237

$\Delta G^\circ_{products} = (-394) + (-237) = -631$ kJ mol^{-1}

$\Delta G^\circ_{reactants} = (-351) + (-157) = -508$ kJ mol^{-1}

$\Delta G^\circ_{rxn} = (-631) - (-508) = -123$ kJ mol^{-1} = $-123{,}000$ J mol^{-1}

The change in standard Gibbs free energy (ΔG°) can be converted to standard potential following equation 3 below:

$$E^o = -\frac{\Delta G^o}{nF} \quad (3)$$

Where n is number of electrons participated in the oxidation of formic acid (n = 2), and F is the Faraday constant (96485 C mol^{-1})

$$E^o = -\frac{(-123{,}000\ J\ mol^{-1})}{2 \times 96485}$$

$$E^o = 0.637\ V\ vs.\ RHE$$

Therefore, a thermodynamic potential 0.639 V vs. RHE was employed for the oxidation of formic acid when calculating the overpotential. The potential in Ag/AgCl scale is changed to reversible hydrogen electrode (RHE) scale following the equation 4 below:

E (vs. RHE) = E (vs. Ag/AgCl) + 0.197 + 0.059 × pH (4)

Table S5. Overpotential values obtained from the difference between applied potential and thermodynamic potential.

$E_{applied\ potential}$ (V vs. Ag/AgCl)	$E_{applied\ potential}$ (V vs. RHE)	Thermodynamic potential (V vs. RHE)	Overpotential (η) (V vs. RHE)
0.01	1.033	0.639	0.394
0.04	1.063	0.639	0.424
0.07	1.093	0.639	0.454
0.1	1.123	0.639	0.484
0.13	1.153	0.639	0.514

A Tafel plot is a plot of overpotential (η) versus log(current density) obtained from the polarization data in the kinetically controlled region of an electrochemical reaction. Mathematically, for instance for anodic reaction is given by:

$\eta = a + blogi$ (1)

Where $a\ is\ intercept\ (a = \frac{2.3RT}{\alpha F} logi_o)$, and b is slope ($b = -\frac{2.3RT}{\alpha F}$, R is the universal gas constant indicated by R (8.314 J mol^{-1} K^{-1}), T is the absolute temperature (298 K), F is the Faraday constant (96485 C mol^{-1}), η is the overpotential, i is the current density, a is the transfer coefficient, and i_o is the exchange current density. A smaller Tafel slope is preferable, as it indicates faster charge transfer kinetics, meaning the current increases rapidly with a small increase in overpotential. The η versus $logi$ provides an intercept of $a = \frac{2.3RT}{\alpha F} logi_o$ and a slope of $= -\frac{2.3RT}{\alpha F}$, implying intercept $= a = -\ blogi_o$. Thus, $logi_o = \ -intercept/slope$. The intercepts from the Tafel plot for $Cu_{98}Ni_2$, $Cu_{95}Ni_5$, $Cu_{92}Ni_8$ and Cu were -0.026, -0.032, -0.055, and -0.062, respectively. Taking the $Cu_{98}Ni_2$ aerogels as an example, the transfer coefficient and exchange current density can be calculated by assuming that one electron participates in the rate-determining step, as follows:

$To\ calculate\ the\ transfer\ coefficient,\ slope = b = -\frac{2.3RT}{\alpha F} = \ -\frac{2.3 \times 8.314 \times 298}{\alpha \times 96{,}485} = 0.0815$

$\alpha = (2.3 \times 8.314 \times 298)/(96{,}485 \times 0.0815) = 0.72$

Similarly, to calculate the exchange current density, we employed the following term;

$$a = \frac{2.3RT}{\alpha F} logi_o$$

$a = -0.026 = \frac{2.3RT}{\alpha F} logi_o = \frac{2.3 \times 8.314 \times 298}{0.72 \times 96{,}485} logi_o$

$a = -0.026 = 0.082 logi_o$

$logi_o = -\frac{0.026}{0.082} = -0.317$

$i_o = 10^{-0.317} = 0.48\ mA/cm^2$

Table S6. Summary of kinetic parameters for formic acid oxidation over all the as-prepared aerogels.

Electrocatalyst	Tafel slope (mV dec^{-1})	Exchange current density (mA cm^{-2})	Charge transfer coefficient	Apparent activation energy kJ mol^{-1}
$Cu_{98}Ni_2$	81.5	0.48	0.72	23.8
$Cu_{95}Ni_5$	84.7	0.42	0.70	26.1
$Cu_{92}Ni_8$	110.1	0..39	0.54	34.4

Cu	126.8	0.32	0.47	36.2

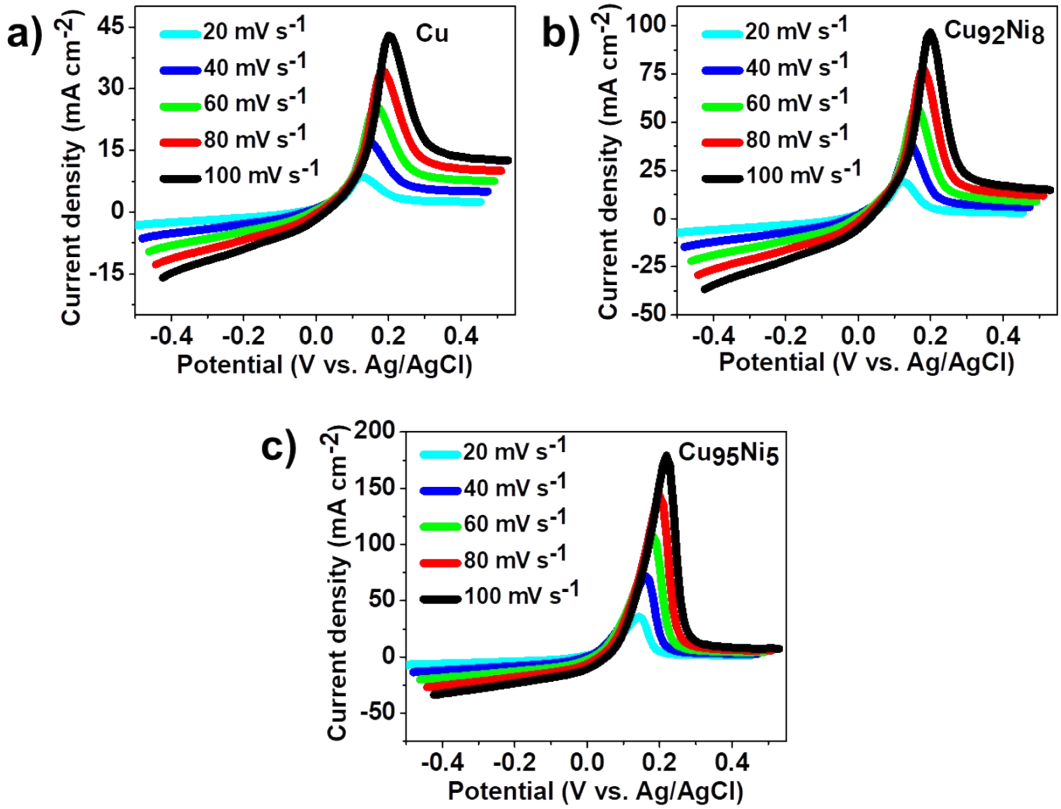

Figure S8. LSV curves of a) Cu, b) $Cu_{92}Ni_8$, and c) $Cu_{95}Ni_5$ aerogels in 1 M KOH + 1 M formic acid at different scan rate.

The activation energy (E_a) in the conventional Arrhenius equation is given by given equation 1 to 4 below:[10, 11]

$$k(T) = Ae^{-E_a/RT} \quad (1)$$

$$lnk(T) = lnA - \frac{E_a}{RT} \quad (2) \quad or$$

$$2.303logk(T) = 2.303logA - \frac{E_a}{RT} \quad (3)$$

$$logk(T) = logA - \frac{E_a}{2.303RT} \quad (4)$$

where A is a pre-exponential factor, k(T) is a rate constant, and R and T are gas constants and temperature, respectively. In a conventional Arrhenius equation, a plot of $logk(T)$ versus reciprocal of temperature provides a slope $= -E_a/2.303R$. The apparent activation energy

(Ea(app)) can be determined from the slope of the Arrhenius plot, which is created by plotting the logarithm of the measured currents at different temperatures against the reciprocal of those temperatures (lni versus 1/T or $logi$ versus 1/T):[10, 11]

$$E_{a(app)} = -2.303R\left[\frac{dlogi}{d(1/T)}\right] = -2.303R \times slope \; or$$

$$E_{a(app)} = -R\left[\frac{dlni}{d(1/T)}\right] = -R \times slope$$

From lni versus 1/T plots (Figure 7c and Figure S9), the slopes were found to be −2868, − 3137, 4133, and − 4356 J mol^{-1} for $Cu_{98}Ni_2$, $Cu_{95}Ni_5$, $Cu_{92}Ni_8$, and Cu, respectively. Thus, the apparent activation energy is given by:

$$E_{a(app)} = -R\left[\frac{dlni}{d(1/T)}\right] = -R \times slope$$

Taking the $Cu_{98}Ni_2$ electrocatalyst as an example, the apparent activation energy was calculated to be $E_{a(app)} = -R \times slope = -8.314 \times -2868 = 23{,}844$ J mol^{-1} = 23.8 kJ mol^{-1}

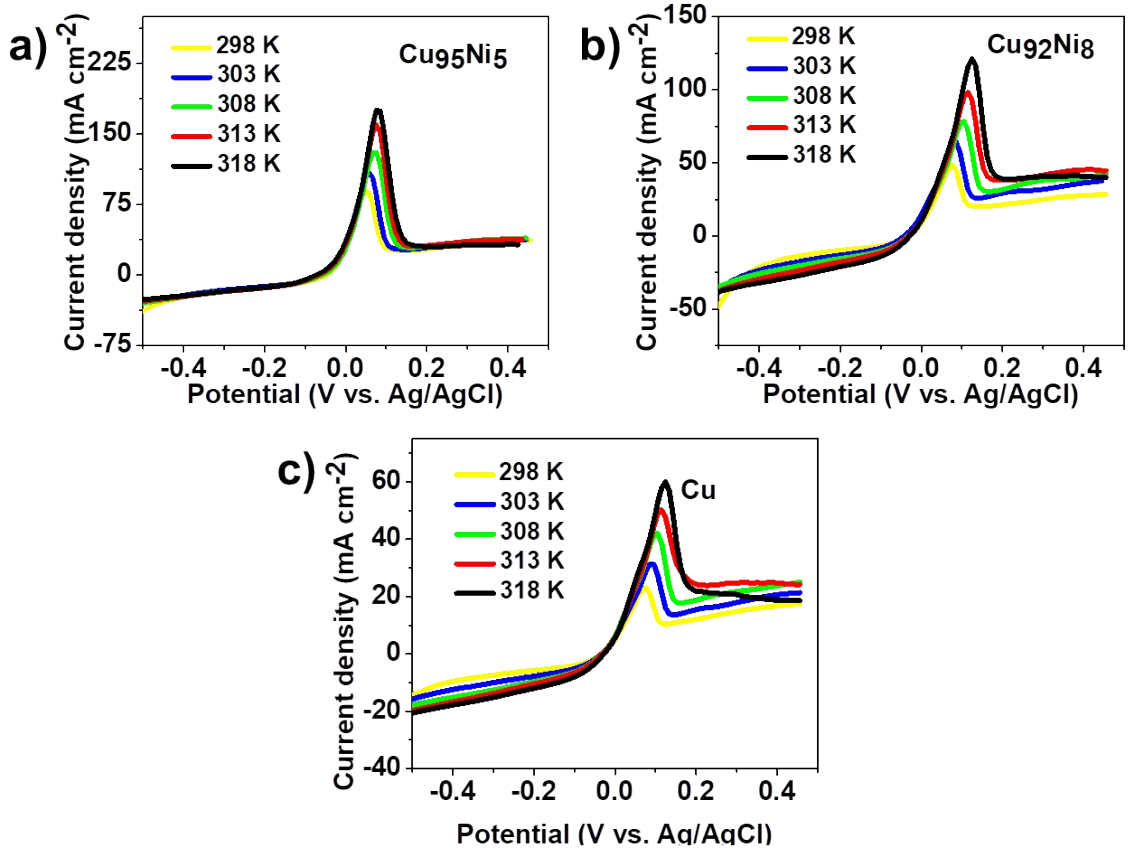

Figure S9. LSV curves of Cu, $Cu_{95}Ni_5$, and $Cu_{92}Ni_8$ aerogels in 1 M KOH + 1 M formic acid at different temperature at 50 mV s^{-1}

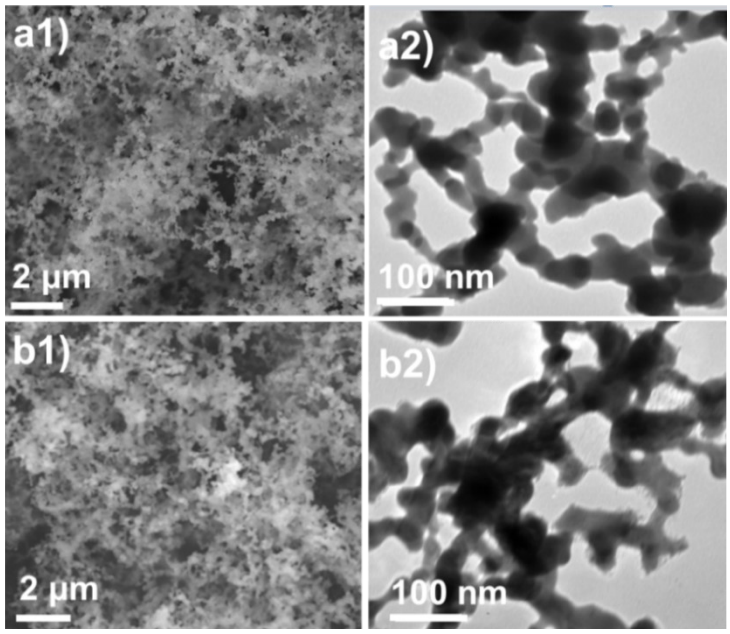

Figure S10. a1) SEM image and a2) TEM images of $Cu_{98}Ni_5$ aerogel before electrocatalysis; b1) SEM image and b2) TEM images of $Cu_{98}Ni_5$ aerogel after electrocatalysis.

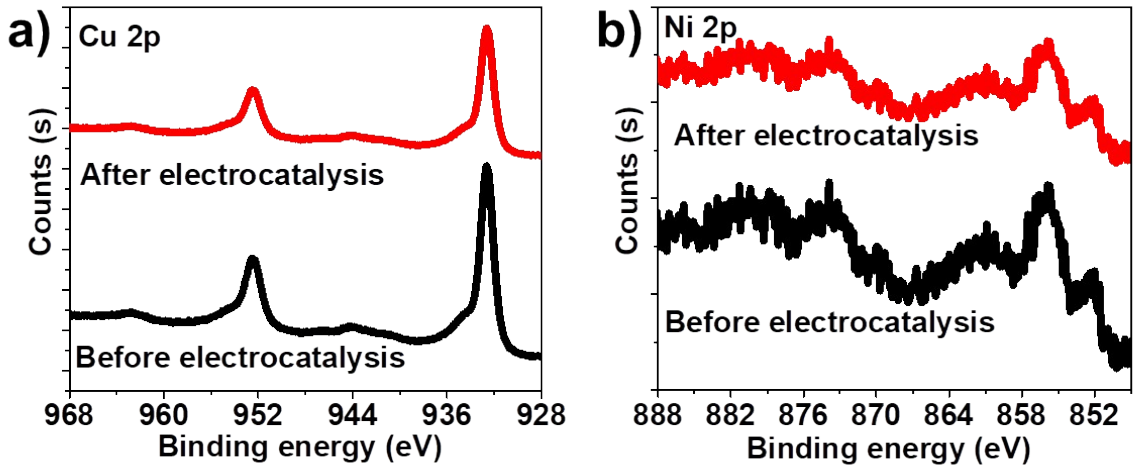

Figure S11. XPS spectra of a) Cu 2p, and b) Ni 2p spectra for $Cu_{98}Ni_5$ aerogel before and after electrocatalysis.

Table S7. Catalaytic activities of non-noble metal electrocatalysts towards formic acid oxidation reaction in basic solution.

S.N	Electrocatalyst	Electrolyte	Activity				Stability	Ref.
			Scan rate ($mV\ s^{-1}$)	A g^{-1}	mA cm^{-2}	Onset potential		
1	Pt_3Ni–C	0.5M H_2SO_4 + 0.5M HCOOH	50 mV/s	~195	-	0.05 V vs. SCE	25% activity retention after 2400s, at 0.3 V vs.SCE	[12]
2	Pd/FeP-250	0.5 M H_2SO_4 + 0.5 M HCOOH	50 mV/s	1540	19.6	0.14 V vs. RHE	~25% activity retention after 3600s, at 0.1 V vs. RHE	13
3	AuPt-24	0.5 M HCOOH + 0.5 M H_2SO_4 (N_2-saturated)	50 mV/s	1.94	7.89	0.3 V vs. RHE	~≈ 34.4 % activity retention after 3600s, at 0.61 V **vs.** RHE	14
4	Pt/BGA	0.5 M H_2SO_4 + 0.5 M HCOOH	20 mV/s	-	5.57	~0.25 V **vs.** Ag/AgCl	NA	15
5	(Y-Pt)-$PtTe_2$ HPNT/C	0.5M H_2SO_4 + 0.5M HCOOH	50 mV/s	6.4	5.4	~0.25 V vs. RHE	80.4% current retention after 32,400s, at 0.4V vs.RHE	16
6	SnO_2@Pd NCs	0.5 M HCOOH + 0.1 M $HClO_4$	50 mV/s	2.46	-	0.15 V vs. RHE,	NA	17
7	Pd@CP	0.1M H_2SO_4 + 0.1M HCOOH	10 mV/s	210.3	1.0	~0.1–0.2 V vs. Ag/AgCl	33.0 % current retention After 3600s, at 0.4 V vs. Ag/AgCl	18
8	p-PtIrBi NPs/C	0.1 m $HClO_4$ + 0.5 m HCOOH	50 mV/s	8.2	18.2	116 mV vs. RHE	55.9 % current retention After 5000s, at 0.3 V vs. RHE	19
9	PdNiP-H	0.5 M H_2SO_4 + 0.5M HCOOH	50 mV/s	1.454	1.985	-0.46V vs. RHE	12.5% current retention After 3500s, at 0.314 V vs RHE	20
10	Pd-1.5	0.5 M H_2SO_4 + 0.5M HCOOH	50 mV/s	634	~20.7	~0.85 V vs RHE	95.3 % current retention after 1000s, at 0.1 V vs RHE	21
11	Net-Pd-HEAA	0.5 M H_2SO_4 + 0.5M HCOOH	50 mV/s	5.94	8.94	~0.10 V vs RHE	92.93% activity retention after 5000s, 0.3 V vs RHE	22

12	B-PdCuAu NAs	0.5 M H_2SO_4 + 0.5 M HCOOH	50 mV/s	1.21	2.29	≈ 30–50 mV	~18.75 % activity retention after 2000 s at 0.3 V vs. Ag/AgCl	23
13	Pd_3P PNTs	0.5 M H_2SO_4 + 0.5 M HCOOH	50 mV/s	360.2	70.1	0.11 V vs. RHE	10.37% activity retention after 10,000s, at 0.7 V vs. RHE	24
14	Pt_2–$PtTe_2$ HJNSAs/C	0.5 M H_2SO_4 + 0.5 M HCOOH	50 mV/s	6.1	8.4	~0.4 V vs. RHE	~ 26.8 % activity retention after 4000s, at 0.6 V vs. RHE	25
15	PdFe/C HT_2	0.1 M HCOOH + 0.1 M $HClO_4$	20 mV/s	352.64	18.97	0.3 V vs RHE	20.72% activity retention after 3600s, at 0.40 V vs. RHE	26
16	Pd_7/R	50 μM H_2SO_4 + 0.5 M HCOOH	10 mV/s	37.7	≈ 0.151	0.1 V vs. Ag/AgCl	NA	27
17	Pt_3Cu_1NW	1.0 M HCOOH +1.0 M $HClO_4$	20 mV/s	-	2.69	~0.6 V vs RHE	NA	28
18	a-FeOx/CoOx/Pt	0.3 M HCOOH	100 mV/s	-	16.4	− 114 mV (vs. Ag/AgCl)	~ 9.32 % activity retention after 12,600s at 50 mV vs. Ag/AgCl	29
19	Pd/1N-CQDs-SiO_2–4rGO	0.5 M H_2SO_4 + 0.5 M HCOOH	50 mV/s	0.951	13.47	≈0.05–0.10 V vs. Ag /AgCl	≈ 21.9 % activity retention after 3600s, at 0.2 V (vs Ag/AgCl)	30
20	Pd/CeO_2	0.5 M H_2SO_4 + 0.5 M HCOOH	50 mV/s	4161.72	9.17	30V mV vs. RHE	79.9% activity retention after 40,000s, at ~0.4 V vs. RHE.	31
21	$PtTe_2$ NSs/C	0.5 M H_2SO_4 + 0.5 M HCOOH	50 mV/s	3.6	14.3	~0.15–0.20 V vs. RHE.	~16.5 % activity retention after 2 000 s , at 0.6 V vs. RHE.	32
22	meso-Pd-B	0.5 M H_2SO_4 + 0.5 M HCOOH	50 mV/s	1310	5.43	~0.05–0.15 V vs. SCE	~ 22 activity retention after 3600s, at 0.25 V vs. SCE	33
23	CuNi@Pt–Cu nano-octahedra/C	0.1 M $HClO_4$ + 0.2 M HCOOH	50 mV/s	3.57	25.2	0.45 V vs. Ag/AgCl	83% activity retention after 3600s, at 0.72 V vs. Ag/AgCl	34

24	Pd/Ti/Pd	0.5 M H_2SO_4 + 0.5 M HCOOH	50 mV/s	0.56	-	~1.5 V vs. RHE	NA	35
25	PdCN-P-200	0.5 M H_2SO_4 + 0.5 M HCOOH	50 mV/s	2.503	6.265	≈ 0.08 – 0.10 V vs. RHE	~21% activity retention after 3600s, at ~ +0.37 V vs. RHE	36
26	PdCu ANCs alloy	0.5 M H2SO4 + 0.5 M HCOOH solution	50 mV s-1 for 6 cycles	554.53 mA mg $_{Pd}^{-1}$	-	0-1.2 V (vs RHE)	88.6% retention of the initial current density After running for 44 000 s	37
27	Ultrathin PdCu Alloy	0.5 M H2SO4 + 0.25 M FA	50 mV/s	1655.7 ± 74.6 mA mg^{-1}_{Pd}	139.8 ± 14.9 m2 g_{Pd}^{-1}	Vs Ag/AgCl	N/A	38
28	Net-Pd-HEAA	0.5 m H2SO4+ 3 m HCOOH	50 mV/s	5.94 A mg_{Pd}^{-1}	-	~ 1.4 V vs NHE	92.93% (5.52 A mgPd−1) of the initial value	39
29	Ultrathin PdAg nanosheets	0.5 M H_2SO_4 + 0.5 M HCOOH	50 mV s^{-1}	987 mA mg^{-1}	50.1 A m^{-2}	0.3 V *vs* SCE	N/A	40
30	$Cu_{98}Ni_2$	1 M KOH + 1 M FA	50	572	142	0.045 V vs. RHE	82% activity retention after 10 h, at 0.1 V vs. Ag/AgCl	This study

References:

1. C. Wang, H. Shang, J. Li, Y. Wang, H. Xu, C. Wang, J. Guo and Y. Du, *Chem. Eng. J.,* 2021, **420**, 129805.
2. K.-R. Yeo, H. Kim, K.-S. Lee, S. Kim, J. Lee, H. Park and S.-K. Kim, ***Appl. Catal. B-Environ. Energy****,* 2024, **346**, 123738.
3. L. Wang, Y. Li, Q. Sun, Q. Qiang, Y. Shen, Y. Ma, Z. Wang and C. Zhao, *ChemCatChem*, 2019, **11**, 2011-2016.
4. Z. Zhuang and W. Chen, *J. Colloid Interface Sci.*, 2019, **538**, 699-708.
5. A. Petričević, V. D. Jović, M. N. Krstajić Pajić, M. Marzec, M. Gajewska, P. Zabinski and N. R. Elezović, *Transactions of the IMF*, 2023, **102**, 91-97.
6. D. Valencia, C. Zenteno, P. Morales-Gil, L. Díaz-García, D. Gómora-Herrera, E. Palacios-González and J. Aburto, *New J. Chem.*, 2020, **44**, 2435-2441.
7. S. J. Folkman, J. González-Cobos, S. Giancola, I. Sánchez-Molina and J. R. Galán-Mascarós, *Molecules*, 2021, **26**, 4756.
8. W. Li, H. Tian, L. Ma, Y. Wang, X. Liu and X. Gao, ***Mater. Adv.***, 2022, **3**, 5598-5644.
9. A. Ali, M. Qasim, S. Sakhi, G. Maduraiveeran and A. S. Alnaser, *Mater. Today Sustain.,* 2025, **30**, 101089.
10. L. V. Kumar, S. Addo Ntim, O. Sae-Khow, C. Janardhana, V. Lakshminarayanan and S. Mitra, *Electrochimica Acta*, 2012, **83**, 40-46.
11. A. F. B. Barbosa, V. L. Oliveira, J. van Drunen and G. Tremiliosi-Filho, *J. Electroanal. Chem.,* 2015, **746**, 31-38.
12. M. Kiani, A. Mahmood, M. Ur Rehman, X.-Q. Tian and A. Saleem, *Hybrid Adv.*, 2025, **10**, 100411.
13. Y. Bao, H. Liu, Z. Liu, F. Wang and L. Feng, *Appl. Catal. B Environ.*, 2020, **274**, 119106
14. X. Li, J. Zhang, C. Jin, B.Yan, J. Cai, M. Li, X. Peng, and Y. Wang, *ACS Sustain. Chem. Eng.*, 2021, **9**, 11062−11069.
15. M. S. Çőgenli and A. B. Yurtcan, *Int. J. Hydrogen Energy*, 2020, **45**, 650–666.
16. X. Lin, S. Geng, X. Du, F. Wang, X. Zhang, F. Xiao, Z. Xiao, Y. Wang, J. Cheng, Z. Zheng, X. Huang and L.Bu, *Nat. Commun.*, 2025, **16**, 1–14.
17. C. Rettenmaier, R. M.Arán-Ais, J. Timoshenko, R. Rizo, H. S. Jeon, S. Kühl, S. W. Chee, A. Bergmann, and B. R. Cuenya, *ACS Catal.*, 2020, **10**, 14540–14551.

18. Y. Zhou, Y. Yang, X. Zhu, T. Zhang, D.-d. Ye, R. Chen, and Q. Liao, *Adv. Funct. Mater*., 2022, 32, 2201872.
19. Y. Sun, W. Chen, W. Zhang, Y. Nie, Q. Zhang, L. Gu, M. Luo, and S. Guo, *Adv. Funct. Mater*., 2023, 33, 2303299.
20. H. Cheng, J. Zhou, H. Xie, S. Zhang, J. Zhang, S. Sun, P. Luo, M. Lin, S. Wang, Z. Pan, J. Wang, X. J. Loh, and Z. Liu, *Adv. Energy Mater*., 2023, **13**, 2203893.
21. S. Mondal, S. K. De, T. Ghosh, S. Mondal, M. Manna, and D. Senapati, *Small Sci*., 2025, 5, 2500063.
22. X. Tan, J. Wang, Y. Xiao, Y. Guo, W. He, B. Du, H. Cui, and C. Wang, *Adv. Mater*., 2025, 37, 2414283.
23. H. Wang, X. Qian, S. Liu, S. Yin, Y. Xu, X. Li, Z. Wang, and L. Wang, *Chem. Eur. J*., 2020, 26,2493–2498.
24. T.-J. Wang, Y.-C. Jiang, J.-W. He, F-M. Li, Y. Ding, P. Chen and Y. Chen, *Carbon Energy*., 2022;4:283–293.
25. C. Dong, B. Zhang, H. Song, S. Zhou, J. Ye, H.-G. Liao, L. Dong, X. Huang and L. Bu, *ACS Nano*, 2024, **18**, 10008−10018.
26. Y. S. Kang, D. Choi, J. Cho, H.-Y. Park, K.-S. Lee, M. Ahn, I. Jang, T. Park, H. C. Ham, and S. J. Yoo, *ACS Appl.Energy Mater*., 2020, **3**, 4226−4237.
27. A. Lal, H. Porat,A. Dutta, D. C.Sesu, M. K.Yadav and A. Borenstein, *Energy Fuels*, 2024, **38**, 18930−18939.
28. Y. Li,Y. Yan,Y. He and S. Du, *ACS Appl. Mater. Interfaces*., 2022, **14**, 11457−11464.
29. A. M. Mohammad, B. A. Al-Qodami, I. M. Al-Akraa, N. K. Allam, and H. H. Alalawy, *Sci. Rep.*, 2024, **14**, 18048.
30. S. Saipanya, P. Waenkaew, S. Maturost, N.Pongpichayakul, N. Promsawan, S. Kuimalee,O. Namsar,K. Income,B. Kuntalue, S. Themsirimongkon and J. Jakmunee, *ACS Omega.,* 2022,**7**, 17741–17755.
31. T. Du, Q. Zhou, W. Lu, H. Cui, J. Liu, X. Lin, L. Yu, X. Zhang and F. Yang, *Small*, 2025, 21, 2407510.
32. J. Bao, H. Sun, W. Yan, S. Liu, W. Xu, J. Fan, C. Zhan, W. Liu, X. Huang and N. Chen, *Small Methods*, 2025, 9, 2402155.

33. Y. Mao, W. Li, Z. Tan, J. Feng, Y. Song, L. Zhang, Y. Fang and Z.-A. Qiao, *Small,* 2025, 21, 2502276.
34. C. Li1 , X. Chen, L. Zhang, B. Zhao, C. Woolever-Frost, P. Bharathan, A. Dennett, G. Zhou and J. Fang, *Catal*, 2025,**7**, 1-13.
35. X. Lu, Z. Wang,Y. Yang, S. Liao and X. Lu, *ACS Appl. Mater. Interfaces*, 2021, **13**, 31725−31732.
36. H. Li, J. Yu, Y. Sui, W. Wang, J. Liu, L. B. Sheng, A. Chen, S. Lu and B. Zou, *Adv. Sci*., 2025, 12, 2504469.
37. Q. Liu, Z. Li, X. Zhou, J. Xiao, Z. Han, X. Jiang, G. Fu and Y. Tang, *Adv. Energy Sustainability Res.,* 2022, **3**, 2200067.
38. N. Yang, Z. Zhang, B. Chen, Y. Huang, J. Chen, Z. Lai, Y. Chen, M. Sindoro, A.-L. Wang, H. Cheng, Z. Fan, X. Liu, B. Li, Y. Zong, L. Gu and H. Zhang, *Adv. Mater.*, 2017, **29**, 1700769.
39. X. Tan, J. Wang, Y. Xiao, Y. Guo, W. He, B. Du, H. Cui and C. Wang, *Adv. Mater.,* 2025, **37**, 2414283.
40. Z. Teng, M. Li, Z. Li, Z. Liu, G. Fu and Y. Tang, *Materials Today Energy*, 2021, **19**, 100596.